Generation of local wind pressure coefficients for the design of low building roofs

K. Suresh Kumar[†]

RWDI Inc., 650 Woodlawn Road West Guelph, Ontario, N1K 1B8, Canada

Ted Stathopoulos[‡]

Centre for Building Studies Department of Building, Civil and Environmental Engineering, Concordia University, 1455 de Maisonneuve Blvd. West Montreal, H3G 1M8, Canada

Abstract. This paper presents recent research on the experimental evaluation of wind loads on low buildings and the recommendations provided in the form of traditional codification. These mainly include the wind loads on buildings with geometries different from those examined in previous studies. This is followed by the evaluation of simulated wind loads on low building roofs. The overall application of a recently proposed simulation methodology for codification purposes is discussed in detail. The traditional codification provides for a group of roof geometries a single peak design pressure coefficient for each roof zone considering a nominal worst-case scenario; this may often lead to uneconomical loads. Alternatively, the presented methodology is capable of providing peak pressure coefficients corresponding to specific roof geometries and according to risk levels; this can generate risk consistent and more economical design wind loads for specific roof configurations taking into account, for instance, directional design conditions and upstream roughnesses.

Key words: codification; design loads; low buildings; pressure; wind.

1. Introduction

Wind loads on low buildings have received recently more attention than in the past, partly because of the large investment associated with these structures and partly because of the disastrous effects imposed on them by recent hurricanes on various locations. The latter have cost insurance industries unprecedented amounts due to the highly increased number of buildings built near the coastal areas severely hit by the intense storms whose frequency seems also to be increasing. Consequently, a renewed interest in the evaluation of wind loads has already generated additional knowledge in comparison to that produced in the previous couple of decades.

Recent studies on the evaluation of wind pressure coefficients have led or will lead to the updating of the North-American wind codes and standards. Such updates relate with the re-examination of wind-induced pressures on gable-roof low buildings with intermediate roof angles (10°-30°), the introduction of pressure coefficient provisions for hip roofs etc. The National Building Code of

---

† Senior Engineer
‡ Professor

Canada (NBCC 1995) currently includes provisions for stepped, multi-gabled (folded), monoslope and sawtooth roof shapes whereas guidelines are provided for hip roofs with roof angles varying from 10° to 30°. The latter are based on a study by Meecham *et al*. (1991) which found that the worst peak pressure on the hip roof was reduced by as much as 50% from that on the gable roof but the study was based on a single roof pitch of 18.4^o. Furthermore, a more recent wind tunnel study by Xu and Reardon (1998) examined three hip-roofed building models of 15°, 20° and 30° roof angle (α) and found that the roof pitch does affect both the magnitude and distribution of hip roof pressures. The 30° hip roof experiences the highest peak suction at roof corner among the three tested hip roofs but the worst peak suctions were much smaller on the hip roofs than on the gable roofs for 15° and 20° roof angles; however, the worst peak suctions on the hip and gable roofs are almost the same for 30° roof angle. Questions have been raised regarding the appropriateness of having a single set of provisions for gable roofs with intermediate slopes for roof angles 10° to 30°. This is due to the fact that over this roof angle range, the wind flow over the building roof may change drastically in comparison to the much more well-defined low and high roof slope ranges. For instance, depending upon the exact value of roof slope, a given roof region could be subjected to either positive or negative pressure. Furthermore, the current provisions for this intermediate roof range have originated from extensive wind tunnel tests on only one roof slope, namely $4:12$, corresponding to a roof angle of 18.4^o and therefore, they may not be appropriate for the entire range. In view of these concerns, a recent wind tunnel study was undertaken by Wu, Wang and Stathopoulos (1998), who performed extensive tests on both local and area-averaged loads. The detailed analysis of the data did not demonstrate the need to specify different design pressure coefficients for each roof angle, as it happens in the Australian Standard (1989). For instance, the data for $\alpha = 15^o$, 20° and 25° can be expressed by a single set of specifications. However, it was clear that the $\alpha = 10^o$ case data would fit better in the intermediate roof slope provisions, whereas the $\alpha = 30^o$ case data would be much better represented by the 30° to 45° range. In addition, a somewhat different set of codal provisions in terms of design pressure coefficients ($CpCg$) for roofs with $10^o \leq \alpha < 30^o$ reflecting more accurately the new experimental findings has been formulated. This is presented in Fig. 1 along with the current provisions and critical values of the experimental data. It has been estimated that the new provisions increase the design pressure coefficients by an overall average of about 15%.

Progress has also been made in the evaluation of wind loads by utilizing computer simulation of wind pressures. This contributes to the recent development towards the new generation of standards (Suresh Kumar and Stathopoulos 1997, 2000, Gioffre *et al*. 1999). The recently proposed simulation methodology in generating Gaussian and non-Gaussian wind pressure on roofs developed by Suresh Kumar and Stathopoulos (1997) can generate numerous samples of similar pressure time series leading to the appropriate selection of peaks with a prespecified probability of exceedance (risk). A systematic wind tunnel study consisting of measurements of wind-induced pressures on low building roofs under various conditions has been utilized to demonstrate the effectiveness of this method. This paper attempts to generalize the simulation methodology by showing the applicability of this approach to derive suitable design pressure coefficients on specific roof configurations taking into account, for instance, directional design conditions and upstream roughnesses. At the same time, current difficulties and areas in which much more research is required are also discussed.
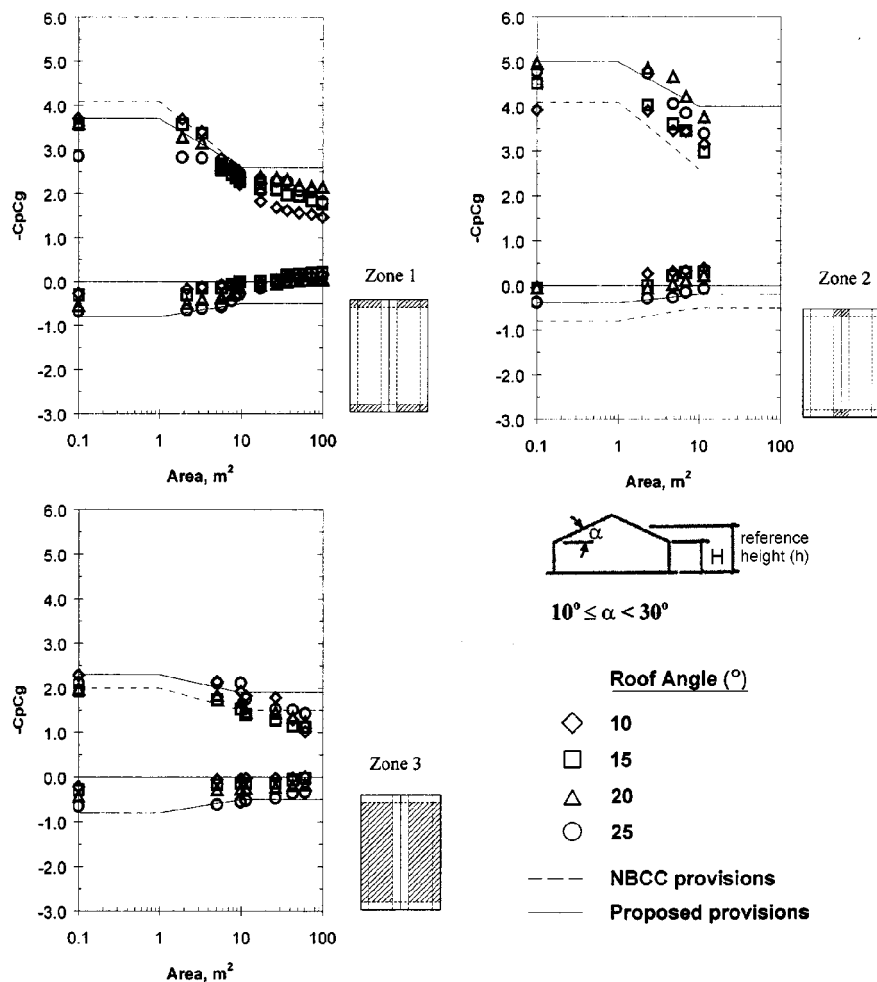
Fig. 1 Most critical pressure coefficients, current NBCC and proposed codal provisions

2. Computer simulation of wind pressures: Background

Wind tunnel and field experimentation are the traditional approach for the investigation of wind-induced pressure fluctuations and time histories. However, the collection of long time histories of wind and pressure data might be time consuming and laborious, considering the inherent variability in such time histories affected by building geometry, measurement location, surroundings and other factors. Alternatively, this can be efficiently handled by computer simulation using probabilistic/statistical models. Gaussian wind pressure fluctuations can be simulated using (1) methods based on Fourier Series (wave superposition), and (2) methods based on the application of an appropriate (analytical) filter subjected to simulated white noise process (linear filtering). A detailed description of the above mentioned simulation techniques has been presented by Grigoriu (1995). Though the Fast Fourier Transform (FFT) algorithm improves the computational efficiency of the wave superposition method, computer memory requirements may be excessive depending on the size of the problem (Kareem 1993). A typical pertinent application of linear filtering techniques is the simulation of wind

pressure fluctuations on monoslope roofs by using an **A**uto-**R**egressive (AR) model of order one (Stathopoulos and Mohammadian 1991). Despite the advantages of ARMA-based simulation over FFT-based simulation, the difficulty remains in the selection of proper model. Moreover this method provides stationarity based on time increment while the FFT-based approach provides unconditional stationarity (Brockwell and Davis 1991).

   Non-Gaussian wind pressure fluctuations can be simply generated using **A**uto-**R**egressive **M**oving **A**verage (ARMA) models but replacing Gaussian with non-Gaussian white noise residuals. An AR model of order one with lognormal residuals has also been applied to overcome the underestimation of peak pressure coefficients on corners of monoslope roofs caused by the Gaussian assumption; however, the improvement over the prediction of peak values was only marginal (Mohammadian 1989, Stathopoulos and Mohammadian 1991). One of the widely recommended methods of simulating non-Gaussian time series is to generate Gaussian time series using either ARMA or FFT model followed by a nonlinear static transformation from Gaussian to non-Gaussian. In a recent paper by Gurley *et al.* (1996), correlation distortion method based on a given target spectrum or autocorrelation as well as modified direct transformation method based on a given sample time history have been presented; both methods used Hermite polynomial transformation. However, these methods are not only complex and iterative in nature but also have difficulty in converging the solution as well as in retaining the original characteristics of spectra due to forward and backward transformation. A promising approach for simulating wind pressure fluctuations of non-Gaussian nature with the help of FFT and AR models has also been introduced (Seong and Peterka 1993, Seong 1993). Most recently, several classes of non-Gaussian processes and their simulation procedures have been described by Grigoriu (1995).

   In summary, the methods for simulating stationary Gaussian as well as non-Gaussian time series can be broadly classified as following either ARMA or FFT methodologies. The ARMA approach is based on the simple and well-known theory of linear difference equations and is computationally efficient. However, ARMA models cannot represent data exhibiting sudden spikes of very large amplitude at irregular intervals and having negligible probability of very high level crossings (Tong 1990); therefore, these are not suitable to represent non-Gaussian time series. On the other hand, the FFT-based approach is the most wide-spread methodology in engineering applications due to its ease in understanding, simplicity and interaction between time and frequency domains. Although the FFT method is not as efficient as ARMA in computational aspects, recent applications of this method for the simulation of non-Gaussian pressure fluctuations as well as perpetual advancement in high-speed computers provide considerable amount of optimism to continue research in this area.

   Recently, wind tunnel measurements focusing on stochastic characteristics of the roof pressure fluctuations were carried out in the boundary layer wind tunnel of the Centre for Building Studies (CBS) of Concordia University (Suresh Kumar 1997). Models of flat, gable (roof angle = 19°) and monoslope roof (roof angle = 15°) buildings 12-15 m high in full scale were tested for several wind angles in open and suburban terrain conditions. Based on these measurements, research work carried out subsequently by the authors has led to the computer simulation of wind pressure fluctuations acting on roofs of rectangular low buildings exposed to various upstream terrain roughnesses (Suresh Kumar and Stathopoulos 1997). The simulation can generate numerous samples of similar pressure time series leading to the appropriate selection of peaks with a pre-specified probability of exceedance (risk). Such records can also be very useful for fatigue design purposes (Suresh Kumar and Stathopoulos 1998b). Both Gaussian and non-Gaussian pressure coefficients have been considered. For the case of Gaussian pressure coefficients, normalized spectra as well as mean and variance of

pressures are required. The standard shapes of spectra for various zones of low building roof geometries (flat, gable and monoslope) have been established and can be used to generate synthetic spectra with the help of variance of pressure fluctuations (Suresh Kumar and Stathopoulos 1998a). For the case of non-Gaussian wind pressure coefficients, in addition to the previous statistical characteristics, a single parameter b depending on both skewness and kurtosis is required. If the mean, variance, skewness and kurtosis of pressure fluctuations acting on a particular roof location are known, time series at specific locations can be generated using standard spectral shapes. The success of computer simulation in generating limitless amounts of data and the present capacity of storage and access to these data provides a new challenge and potential benefit to design professionals.

3. Representation of wind pressure time series

Gaussian and non-Gaussian loads have significantly different implications in the design process (Grigoriu 1995). In this study, a particular region is considered non-Gaussian if the absolute values of skewness and kurtosis of pressure fluctuations at various taps are greater than 0.5 and 3.5 respectively. In order to show concisely the distinct characteristics of pressures at various roof regions and, most importantly, to model the roof pressure characteristics efficiently, typical roof geometries have been classified into zones of Gaussian and non-Gaussian pressure fluctuations for ranges of wind direction by utilizing the large amounts of measured data (Suresh Kumar and Stathopoulos 1998a). The approximate Gaussian and non-Gaussian regions of flat, gable and monoslope
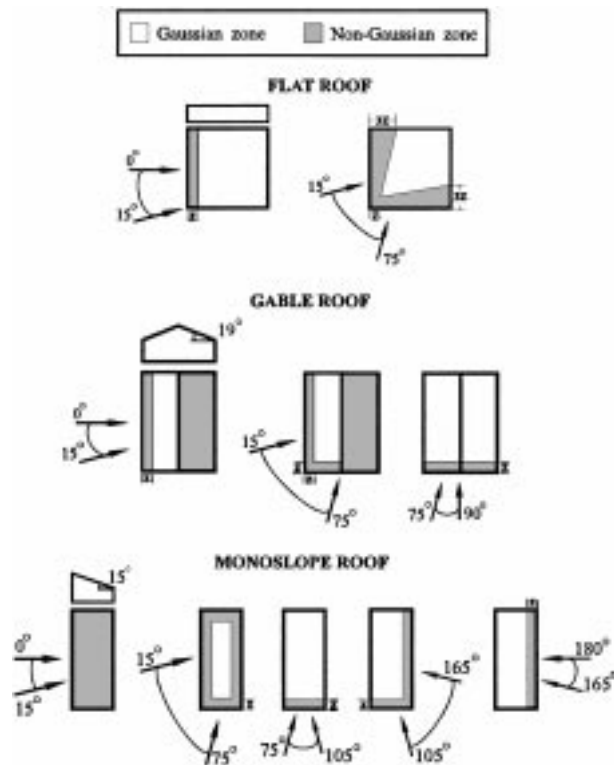

Fig. 2 Gaussian and non-Gaussian roof zones

roofs are provided in Fig. 2; variable z is assumed to be 10% of least horizontal dimension or 40% of lower eave height whichever is less (NBCC 1995). In general, windward edges of roofs are subjected to non-Gaussian fluctuations.

A general approach based on Fast Fourier Transform (FFT) algorithm has been developed to represent Gaussian and non-Gaussian local roof pressure characteristics (Suresh Kumar 1997, Suresh Kumar and Stathopoulos 1997). This method is set to preserve the second order characteristics (variance, spectral density function) through the amplitude part of the Fourier transform and the spike features by properly tailoring the phase part of the pressure fluctuations. The particular spike features inducing the non-Gaussian character to the pressure fluctuations have been achieved by preserving the target skewness and kurtosis. The development and full details of this method can be found in Suresh Kumar and Stathopoulos (1999). The simulation procedure requires the knowledge of both Fourier amplitude and phase in order to generate pressure time series. The Fourier amplitude is constructed from power spectra of the pressure fluctuations. In case of non-Gaussian wind pressures, a simple stochastic model with a single parameter b, inducing non-normality in time series has been suggested for the simulation of phase; whilst, phase part of Gaussian wind pressures has been represented by independent identically distributed uniform random numbers ranging from $-\pi$ to π. Many successful simulations have been performed at various locations of the roof (Suresh Kumar 1997).

The schematic of the simulation of Gaussian time series using power spectra is shown in Fig. 3; where, $S_m(f_k)$ corresponds to mathematical spectrum, f_k corresponds to frequency, Δf corresponds to frequency resolution, n corresponds to time series length, $\sqrt{I_k}$ corresponds to Fourier amplitude, ϕ_k
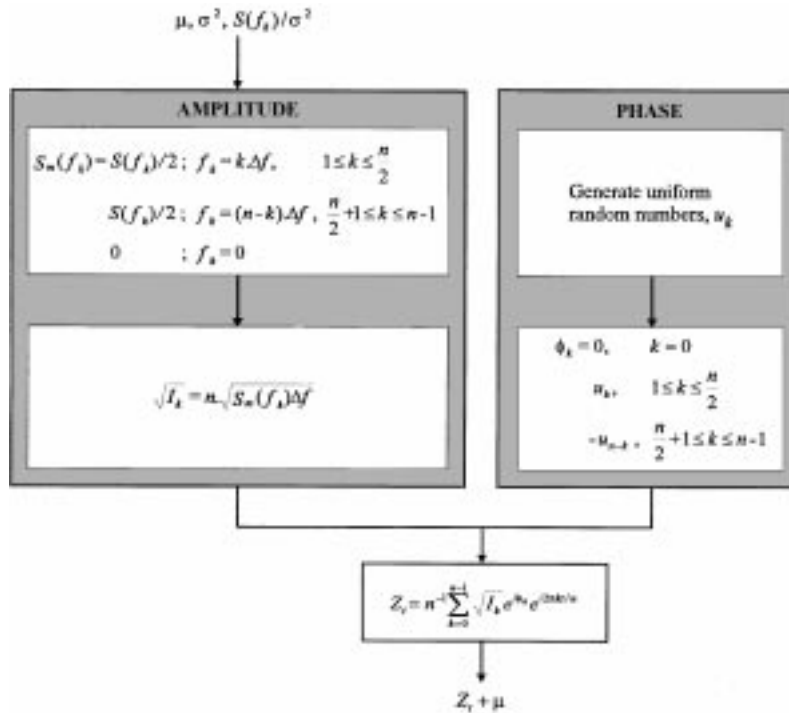

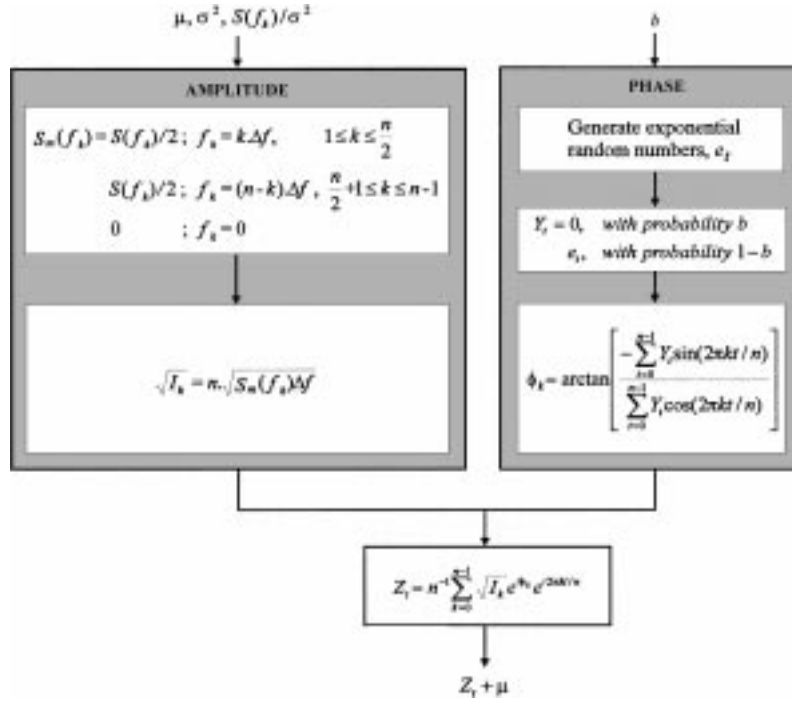Fig. 3 Schematic of the generation of Gaussian wind pressure time series

Fig. 4 Schematic of the generation of non-Gaussian wind pressure time series

corresponds to Fourier phase, Z_t corresponds to time series and the term $2\pi k/n$ is the integer multiple of the fundamental frequency $2\pi/n$ known as Fourier frequency. Mean (μ), variance (σ^2) and normalized physical spectrum ($S(f_k)/\sigma^2$) of the pressure fluctuations are the required inputs for the simulation. Using this procedure, a number of samples of time series having the same spectral density function, variance and mean can be generated. The simulation methodology for non-Gaussian fluctuations emphasizes the generation of phase part, which induces the non-normality in time series. Fig. 4 shows a schematic of the simulation of non-Gaussian time series; Y_t corresponds to skeleton time series, b is the probability parameter which controls the frequency of spikes in the skeleton time series and the intensity of spikes in the synthetic time series, and e_t is the exponential random number. Mean (μ), variance (σ^2), normalized physical spectrum ($S(f_k)/\sigma^2$) and parameter b of the pressure fluctuations are the inputs required for this simulation. The parameter b induces the target skewness as well as kurtosis in a time series through phase tailoring. The details of the estimation of parameter b as well as simulation of non-Gaussian time series have been described elsewhere (Suresh Kumar 1997, Suresh Kumar and Stathopoulos 1999). It is sufficient here to note that the computation of parameter b is accomplished by minimizing the sum of the squared errors in higher-order statistics such as skewness and kurtosis. The stationarity of the simulated time series has also been justified for $b \leq 0.9$; fortunately, values of $b > 0.9$ are not obtained even when modeling highly non-Gaussian pressure fluctuations (Suresh Kumar and Stathopoulos 1999).

4. Input

In the present study, the statistics (mean and variance) of the pressure time series obtained from

wind tunnel experiments have been used for the simulations. However, in practice these statistics can be obtained from literature; the values of mean and variance of pressure fluctuations on different locations of common roof geometries for various conditions can be obtained from past studies.

The required Fourier amplitude part in the simulation can be constructed from corresponding spectra. Recent wind tunnel studies have shown that it is possible to categorize normalized spectra on a roof based on their similarities (Suresh Kumar and Stathopoulos 1998a). On this basis, a suitable empirical form has been derived for the synthetic generation of normalized spectra. Finally, after classifying the zones of Gaussian and non-Gaussian pressures due to the difference in simulation methodologies, normalized spectra are categorized and the standard spectral shapes associated with various zones of each roof and their parameters are established. Two spectra were suggested for the non-Gaussian zones of each of the flat, gable and monoslope roof; while one spectrum was suggested for the Gaussian zones of each of the flat and gable roofs and two spectra for the Gaussian zones of the monoslope roof. Each spectrum is assigned a name where the second letter stands for the roof type (F - Flat roof, M - Monoslope roof, G - gable roof), the third stands for the type of region (G - Gaussian, NG - non-Gaussian) and the number (1 or 2) stands for the type of spectra in that zone. Further details of this investigation can be found in Suresh Kumar (1997), Suresh Kumar and Stathopoulos (1998a). For practical purposes, from the knowledge of variance of pressure fluctuations at a specific roof location, spectra of pressure fluctuations can be synthetically generated for the same location using the developed standard spectral shapes.

Skewness and kurtosis of non-Gaussian roof pressures and the associated parameter b values vary depending on the tap location and wind direction. It appears that further classifying these narrow roof zones to assign constant parameter b values is counter-productive. Instead, it may be better to generate the expected variation of skewness and kurtosis with respect to b for each spectrum; this helps to select the value of parameter b satisfying the target skewness and kurtosis of the pressures (Suresh Kumar and Stathopoulos 2000). Such an exercise has been carried out and the results showed similarities in the variation of skewness and kurtosis with respect to parameter b corresponding to different spectra. This indicates the possibility of reducing the number of spectra established for simulations; this is elaborated in the next section. In the present study, the statistics (skewness and kurtosis) of the time series was known from wind tunnel experiments. In practice, the skewness and kurtosis values of pressure fluctuations are seldom known; however, these values can be established by analyzing some limited existing databases of time histories and by carrying out wind tunnel measurements for unavailable configurations.

5. Towards generalization

Many simulations have been carried out using the standard spectral shapes associated with the corresponding tap locations. Details about the evolution of these standard spectral shapes associated with different roof regions are available in Suresh Kumar and Stathopoulos (1998a). Results indicated the capability of the proposed methodology to represent the most pertinent statistics in a simple manner (Suresh Kumar 1997, Suresh Kumar and Stathopoulos 1997).

Based on the similarities found in curves of skewness and kurtosis versus the parameter b for various conditions, it may be appropriate to use a single pressure spectrum in non-Gaussian zones for all roof geometries. Within this context, the simulated skewness and kurtosis values based on previously established spectra for non-Gaussian zones have been shown in Fig. 5 along with the measurements for all roof geometries. For this computation, the b value has been varied from 0 to
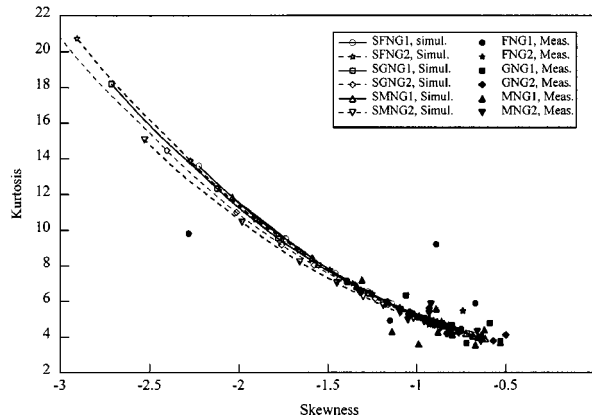
Fig. 5 Simulated and measured skewness and kurtosis values for all roof geometries

0.9 at an increment of 0.01; the values of the other parameters used in simulations are $n = 8192$ and sampling frequency, $f_s = 500$ Hz. The upper limit of b is fixed to satisfy the stationarity requirements (Suresh Kumar and Stathopoulos 1999); while, the increment of 0.01 is set based on the sensitivity of parameter b on simulation results. For each b value, 100 time series have been simulated using the method depicted in Fig. 4 and thereafter, the skewness and kurtosis values have been calculated based on 100 records with an objective to reduce the sensitivity of the different random number sets in repetitive simulations. Note the influence of the types of spectra on the simulated skewness and kurtosis values. Note that irrespective of the different spectra used in simulations, the variations in the curves are negligible especially where the measured data are clustered. Moreover, the measurements show that single pressure spectra can represent the statistics. Note also that the high values of skewness and kurtosis of simulated time series are rarely obtained in the measurements. After an extensive investigation, the spectrum SMNG1 was chosen to represent the spectrum of non-Gaussian fluctuations from all roof configurations. A similar investigation led to the selection of a single spectrum SMG1 for representing Gaussian fluctuations (Suresh Kumar and Stathopoulos 2000a). The proposed spectra SMG1 and SMNG1 are shown in Fig. 6 along with their equation and associated parameters; the abscissa represents the reduced frequency, $F = fh/V$, f is the frequency, h is the mean roof height and V is the mean velocity at mean roof height.

Fig. 7 provides the variation of skewness and kurtosis with respect to b, estimated based on the spectrum SMNG1 as previously mentioned; analytical expressions relating the parameter b with skewness (Sk) and kurtosis (Ku) can also be derived. This diagram can be used to select the parameter b based on the known skewness or kurtosis value of the time series. The two values of b corresponding to skewness and kurtosis are, in most cases, close to each other. In case of difference in b values, select the b value from this range which satisfies the target skewness and kurtosis in the least square sense. The Sum of the Squared Errors (SSE) in skewness and kurtosis (i.e., SSE = (simulated skewness from Fig. 7 - target skewness)^2 + (simulated kurtosis from Fig. 7 - target kurtosis)^2) are calculated for each value of b in this range and the value which gives the least SSE is chosen as the optimum one. This procedure can be easily incorporated in the program. Note that as per Fig. 7, the minimum and maximum absolute skewness values that can be achieved in simulations are 0.6 and 2.05 respectively, whereas the corresponding minimum and maximum kurtosis values are 3.9 and 11.8 respectively. Considering the measured values of skewness and kurtosis - see Fig. 5,
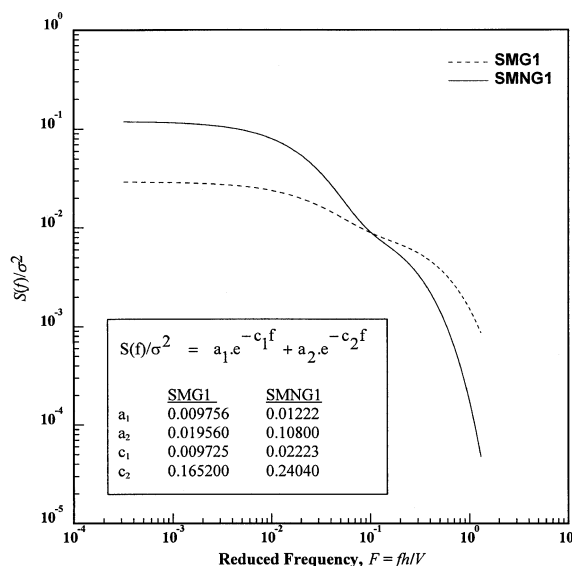
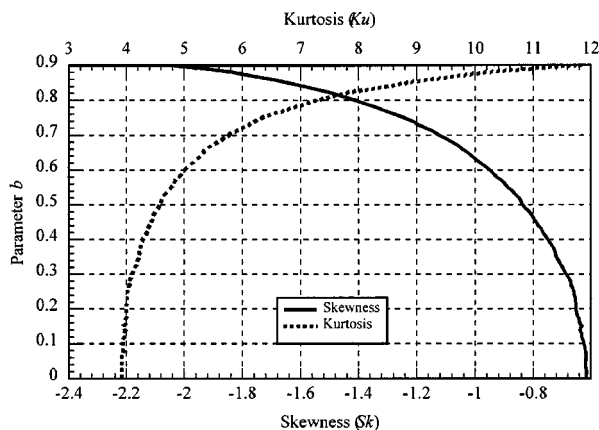Fig. 6 Proposed synthetic spectra for Gaussian and non-Gaussian simulations

Fig. 7 Variation of skewness and kurtosis based on spectra SMNG1

the upper bounds of the achievable skewness and kurtosis in the simulations are satisfactory. However, the lower bounds are slightly above the criterion previously set to distinguish non-Gaussian roof zones, i.e., absolute skewness = 0.5 and kurtosis = 3.5. The value zero is suggested for the parameter b when the absolute value of the target skewness lies between 0.5 and 0.61 and the target kurtosis lies between 3.5 and 3.9; the simulated results may not be very different from the measured data in such cases.

Figs. 8 and 9 show typical results in the form of measured and simulated peak pressure coefficients (Cp_{peak}) versus probability of exceedance for two non-Gaussian cases. All simulations have been carried out using the SMNG1 spectrum and the value of b from Fig. 7. The comparison shows that the simulated suction peaks are close to the measured values; however, differences up to $\pm$ 15% have been found in some cases at individual points. Although the change in spectrum did change
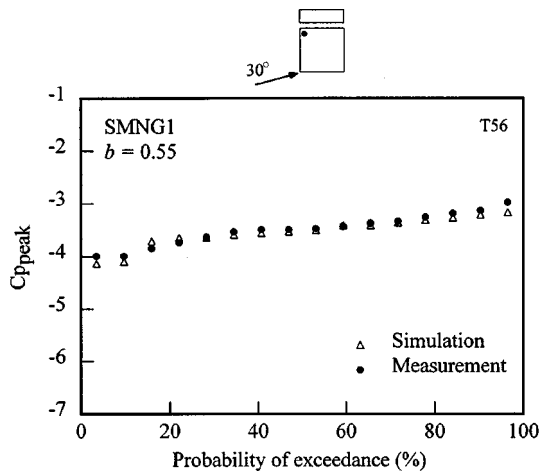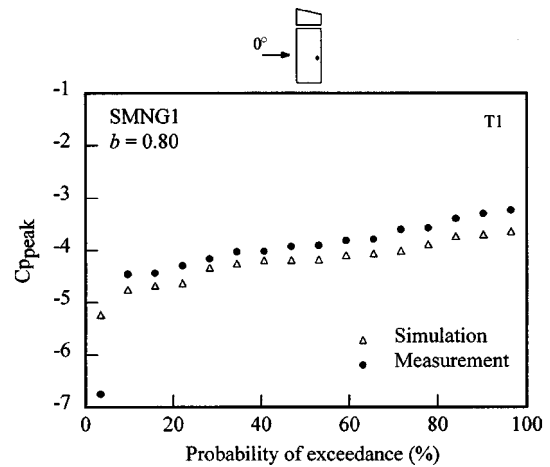
Fig. 8 Extreme pressure coefficients (Flat roof)   Fig. 9 Extreme pressure coefficients (Monoslope roof)

Table 1 Statistics of time series corresponding to Figs. 8 and 9

Sanple		Mean	Variance	Skewness	Kurtosis
T56	Simulation	-1.22	0.13	-0.86	4.64
	Measurement	-1.22	0.13	-0.93	4.69
T1	Simulation	-1.11	0.14	-1.40	7.20
	Measurement	-1.11	0.14	-1.40	7.12

the values of b required for the simulations, clearly, the double change, both in spectrum and the b value did not influence the peak values or statistics substantially. Similar results were found in other cases. Therefore, it appears that a single spectrum can indeed represent the pressure fluctuations in non-Gaussian zones of all roof geometries. Similar results prevail in case of Gaussian simulations using SMG1 (Suresh Kumar and Stathopoulos 2000). The statistics (mean, variance, skewness and kurtosis) of the simulated and target time series based on 16 records shown in Table 1 are close to each other. Diagrams such as those of Figs. 8-9 can be used to establish design pressure coefficients according to any desirable risk level, presumably consistent with reliability-based design.

In summary, the generalized synthesis of the pressure coefficients is presented in Fig. 10. The initial input is mean and variance of the pressure fluctuations and the corresponding roof geometry, tap location and wind direction. With these inputs and the roof zones presented in Fig. 2, the Gaussian or non-Gaussian character of the time history to be simulated can be decided. If it is Gaussian, the corresponding spectra SMG1 (Fig. 6) will be selected for the generation of Fourier amplitude and the Fourier phase will be generated from uniform random numbers. On the other hand, if the zone is non-Gaussian, the corresponding spectrum SMNG1 (Fig. 6) will be selected for the generation of Fourier amplitude and the parameter b will be required for the generation of Fourier phase. In order to estimate b, the target skewness and kurtosis of the pressure fluctuations has to be provided and Fig. 7 can then be utilized. Note that numerous samples having the same statistics and spectrum, which are required to carry out extreme value and fatigue analysis, can easily be generated using this procedure. The complete procedure is programmed in MATLAB environment.
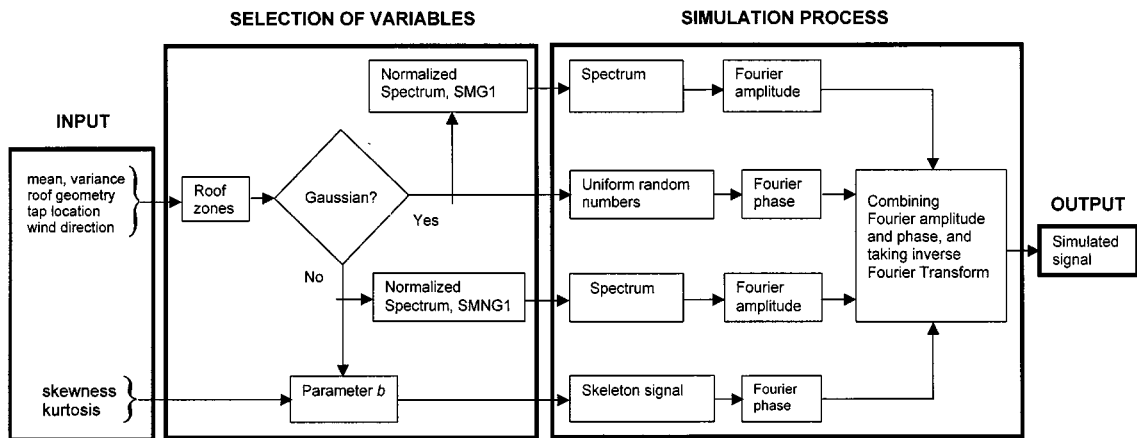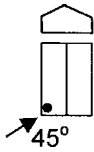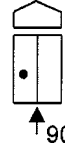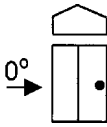
Fig. 10 Generalized synthesis procedure

Table 2 Comparison between alternate and traditional codifications

	Alternate Codification						Traditional Codification		
	Input			**Selection of variables**			**Output**	**Zone** *CpCg*	*CpCg*/0.8
Roof geometry $l = 60.8$ m $b = 39.2$ m $h_1 = 12$ m $\alpha = 19^\circ$	Mean Variance	Skewness Kurtosis	Gaussian? (Fig. 2)	Spectrum (Fig. 6)	b (Fig. 7)			(Fig. 1)	
T37 45°	-0.38 0.16	-1.06 6.35	No	SMNG1	0.75	Skewness = -1.24 Kurtosis = 6.31 Peak = -3.51	1	-4.1	-5.1
T78 90°	-0.31 0.03	-0.07 3.32	Yes	SMG1		Skewness = 0.00 Kurtosis = 3.01 Peak = -0.96	3	-2.0	-2.5
T69 0°	-0.80 0.05	-0.93 5.63	No	SMNG1	0.68	Skewness = -1.09 Kurtosis = 5.53 Peak = -2.40	3	-2.0	-2.5

Note: l = length, b = width, h_1 = lower eave height, α = roof angle

Table 2 compares alternative codification with the traditional codification for specific cases. All the cases refer to the taps on the gable roof shown in Fig. 2. The information such as roof type, tap location and wind direction provided in the second column of the table is used in conjunction with Fig. 2 to decide whether the time series to be simulated is Gaussian or non-Gaussian. In case of

T37, the tap is located on a non-Gaussian zone. Since this is a non-Gaussian case, the spectrum SMNG1 provided in Fig. 6 is chosen for the simulation of the Fourier amplitude part. Skewness and kurtosis are also required as inputs for the estimation of b. These are provided in the second column of Table 2, whereas the parameter b is selected from Fig. 7 by determining the value that minimizes the sum of the squared errors from each of the target skewness and kurtosis values. All the selected variables for this simulation are provided in the third column of this table. The output in the form of skewness, kurtosis and peak are provided in the fourth column of this table; the simulated peak value is the mean of the 16 simulated peaks. As expected, the simulated values are close to the measured values. The second case T78 is Gaussian; therefore, the spectrum SMG1 (Fig. 6) was used for this simulation. Note that the process is not perfectly Gaussian. The output results show that the simulated time histories are Gaussian, thus avoiding the slight non-normality of the actual time series. This may result in slight under-prediction of the peaks; the differences are found to be still within $\pm 15\%$. The third case T69 in Table 2 is, once again, non-Gaussian and the synthesis procedure is similar to the first.

   A similar exercise has been carried out for other roof geometries and similar results were obtained. Further, the fifth column of Table 2 provides the corresponding zone where this tap is located, the associated $CpCg$ value as per NBCC (1995) and the $CpCg$ value divided by 0.8. Note that the $CpCg$ value provided in the code is a direction-independent worst peak pressure coefficient for each zone multiplied by a factor 0.8. In all cases, the simulated peak values are below the worst design pressure coefficients used in the traditional codification process ($CpCg$/0.8). This is encouraging since instead of having a worst peak value, peak values can be tailored for specific cases using this alternative codification procedure. Moreover, the code provides a single peak value compared to the spectrum of risk-consistent peaks that can be obtained with the new procedure. Although, pressure coefficient skewness and kurtosis databases are not currently available and even means and variances of pressure coefficients are still to be organized, the performance of the new codification procedure is, overall, quite promising.

6. Conclusions

   This paper presents the latest developments and the progress made in the evaluation of wind loads on roofs of low buildings. It refers to some of the most recent studies that have led or will lead to the updating of the North-American wind codes and standards. Such updates include the re-examination of wind-induced pressures on gable-roof low buildings with intermediate roof angles (10°-30°) and the introduction of pressure coefficient provisions for hip roofs.

   A new approach towards future codification by generating time histories of pressures acting on low building roofs of specific geometries and for any selected wind direction has been described. The foundation of this approach is the recently proposed general method for the representation of Gaussian and non-Gaussian roof pressure coefficients. This approach leads to more accurate and economical design of buildings since the pressure coefficients specified will be tailored to a given particular case of interest rather than to a generic type of building with enveloped loads, as it is currently the case. Further work is necessary to build appropriate databases for the first four moments (mean, variance, skewness and kurtosis) of the roof pressure fluctuations at various conditions.

References

Australian Standard (1989), Part 2: Wind Loads, Standards Australia, Standards House, 80 Arthur St, North Sydney NSW.

Brockwell, P.J., and Davis, R.A. (1991), *Time Series: Theory and Methods*, Springer Verlag.

Gioffre, M., Grigoriu, M., Kasperski, M. and Simiu, E. (1999), "Wind-induced peak bending moments in low-rise building frames", *10th Int. Conf. Wind Eng*., A.A. Balkema Publishers, Copenhagen, Denmark.

Grigoriu, M. (1995), *Applied non-Gaussian Processes: Examples, Theory, Simulation, Linear Random Vibration and MATLAB Solutions*, Prentice-Hall: Englewood Cliffs, New York.

Gurley, K.R., Kareem, A., and Tognarelli, M.A. (1996), "Simulation of a class of non-normal random processes", *Int. J. Non-Linear Mech*., **31**(5), 601-617.

Kareem, A. (1993), "Simulation of stochastic wind effects", *Proc. 7th US Nat. Conf. Wind Eng*., Los Angeles, USA.

Meecham, D., Surry, D. and Davenport, A.G. (1991), "The magnitude and distribution of wind-induced pressures on hip and gable roofs", *J. Wind Eng. Ind. Aerod*., **38**, 257-272.

Mohammadian, A.R. (1989), "Wind loads on buildings with monosloped roofs: stochastic modelling of wind pressure fluctuations", Ph.D. Thesis, Concordia University, Montreal, Canada.

NBCC (1995), National Building Code of Canada, Associate Committee on the National Building Code, National Research Council of Canada, Ottawa.

Seong, S.H. (1993), "Digital synthesis of wind pressure fluctuations on building surfaces", Ph.D. Thesis, Colorado State University, Fort Collins.

Seong, S.H. and Peterka, J.A. (1993), "Computer simulation of non-Gaussian wind pressure fluctuations", *Proc. 7th US Nat. Conf. Wind Eng*., Los Angeles, CA, U.S.A.

Stathopoulos, T. (1995), "Evaluation of wind loads on low buildings - A brief historical review, A State-of-the-Art in Wind Engineering", International Association for Wind Engineering, Wiley Eastern Limited.

Stathopoulos, T., and Mohammadian, A.R. (1991), "Modelling of wind pressures on monoslope roofs", *Eng. Struct*., **13**, 281-292.

Suresh Kumar, K. (1997), "Simulation of fluctuating wind pressures on low building roofs", Ph.D. Thesis, Concordia University, Montreal, Canada.

Suresh Kumar, K. and Stathopoulos, T. (1997), "Computer simulation of fluctuating wind pressures on low building roofs", *J. Wind Eng. Ind. Aerod*., **69-71**, 485-495.

Suresh Kumar, K. and Stathopoulos, T. (1998a), "Spectral density functions of wind pressures on various low building roof geometries", *Wind and Structures*, **1**(3), 203-223.

Suresh Kumar, K. and Stathopoulos, T. (1998b), "Fatigue analysis of roof cladding under simulated wind loading", *J. Wind Eng. Ind. Aerod*., **77-78**, 171-183.

Suresh Kumar, K. and Stathopoulos, T. (1999), "Synthesis of non-Gaussian wind pressure time series on low building roofs", *Eng. Struct*., **21**(12), 1086-1100.

Suresh Kumar, K. and Stathopoulos, T. (2000), "Alternate codification of wind pressure coefficients for low building roofs", *Annual CSCE Conference*, London, Ontario.

Tong, H. (1990), *Non-Linear Time Series: A Dynamical System Approach*, Clarendon, Oxford.

Wu, H., Wang, K. and Stathopoulos, T. (1998), "Pressure coefficients for gable roofs of intermediate slopes", *Proc. 2nd East European Wind Eng. Conf*., Prague.

Xu, Y.L. and Reardon, G.F. (1998), "Variation of wind pressure on hip roofs with roof pitch", *J. Wind Eng. Ind. Aerod*., **73**, 267-284.